

# Scalable visualisation methods for modern Generalized Additive Models

Matteo Fasiolo<sup>1,†</sup>, Raphaël Nedellec<sup>2</sup>, Yannig Goude<sup>2</sup>, and Simon N. Wood<sup>1</sup>

<sup>1</sup>School of Mathematics, University of Bristol, United Kingdom.

<sup>2</sup>Électricité de France R&D, Saclay, France.

<sup>†</sup>Correspondence: [matteo.fasiolo@bristol.ac.uk](mailto:matteo.fasiolo@bristol.ac.uk)

August 11, 2022

## Abstract

In the last two decades the growth of computational resources has made it possible to handle Generalized Additive Models (GAMs) that formerly were too costly for serious applications. However, the growth in model complexity has not been matched by improved visualisations for model development and results presentation. Motivated by an industrial application in electricity load forecasting, we identify the areas where the lack of modern visualisation tools for GAMs is particularly severe, and we address the shortcomings of existing methods by proposing a set of visual tools that a) are fast enough for interactive use, b) exploit the additive structure of GAMs, c) scale to large data sets and d) can be used in conjunction with a wide range of response distributions. All the new visual methods proposed in this work are implemented by the `mgcViz` R package, which can be found on the Comprehensive R Archive Network.

**Keywords:** Generalized Additive Models; visualisation; electricity load forecasting; residuals checking; regression modelling; interactive model building

## 1 Introduction

The aim of this paper is to propose new visualisation tools for interactive model checking and development in smooth additive models, with a particular focus on large models for big data sets, and model checking beyond simple exponential family regression. We discuss the computational efficiency issues that this entails, and provide illustration of the practical application of many of the plots in the context of model building for electricity load forecasting.

Recent computational developments in GAM fitting methods, such as Wood et al. (2015), Wand (2017) and Wood et al. (2017), have made it possible to use these models to

explore very large data sets. However, visual methods and software have lagged behind, to the point that, for data sets comprising over  $10^6$  observations, GAM model fitting might take less time than rendering basic visual residuals checks. The methods described here address this issue by binning the data and summarising it into a form that can be displayed effectively, as suggested by Wickham (2013). To enable interactive exploration, the new tools aim at handling data sets comprising  $10^7$  to  $10^8$  observations within a few seconds.

Beside faster computation, in the last two decades GAM methods have expanded in terms of the range of models that can be fitted. Indeed, modern GAMs have moved beyond the exponential family, and are not limited to modelling the mean. A major development in this direction has been the introduction of Generalized Additive Models for Location, Scale and Shape (GAMLSS) by Rigby and Stasinopoulos (2005), where all parameters of the response distribution can be modelled via additive functions of the covariates. This allows, for example, fitting GAMs where the mean, variance, skewness and kurtosis of the response distribution depend on the covariates. While this permits greater flexibility, a practitioner is now left with the task of specifying several linear predictors, rather than one. Further, such models are often expensive to fit, which makes performing exhaustive or automated variable selection impracticable. Instead, this paper proposes a set of visual tools intended to aid visual variable selection. In particular, we propose several visualisations aimed at detecting residual patterns and anomalies, and we demonstrate their usefulness in the context of electricity load forecasting. Importantly, the tools quantify the uncertainty of the residual patterns and are applicable to most distributional GAMs.

GAM models can include a variety of smooth terms, and effective visualisation of such effects is essential in the context of load forecasting. Indeed, operational forecasters need to understand the estimated effects, in order to assess their physical plausibility and judge when it may be safe to use the model despite unusual covariate configurations. Good visualisation is key to this, hence this paper also describes new smooth effect plots which permit visual uncertainty assessment and can be manipulated interactively.

## 2 Methodology

We consider additive models that can be fitted using the general framework of Wood et al. (2016). In particular, if we let  $y$  be the response variable, then

$$y_i \sim p_m(y|\boldsymbol{\theta}_i), \quad g_k(\theta_{ki}) = \sum_{j \in \mathcal{S}_k} f_{kj}(\mathbf{x}_i), \quad \text{for } i = 1, \dots, n,$$

where  $p_m(y|\boldsymbol{\theta})$  is a distribution parametrized by  $\boldsymbol{\theta}_i = \{\theta_{1i}, \dots, \theta_{pi}\}$ , the  $f_{kj}$ 's are unknown smooth functions of the covariate vector  $\mathbf{x}$ ,  $g_1, \dots, g_p$  is a sequence of known smooth monotonic link functions and  $\mathcal{S}_k$  is the set of indices specifying on which smooth effects  $\theta_k$  depends. The  $f_{kj}$ 's are constructed using basis expansions of low rank, such as splines, whose complexity is controlled using ridge penalties on the regression coefficients. In the rest of the paper we indicate  $p_m(y|\boldsymbol{\theta})$  with  $p_m(y|\mathbf{x})$ , to make the dependence on  $\mathbf{x}$  explicit.

## 2.1 Software

The visual methods developed here could be applied to GAMs fitted with a variety of software, but for concreteness we focus on the `mgcv` package in the R statistical software. `mgcv` provides tools for building and fitting GAM models including a wide variety of smooth or random effects and response distributions, and it is supplied by default with R. In the last few years the computational scalability of `mgcv` has benefited from the inclusion of the fast fitting methods of Wood et al. (2015, 2017). Further, since version 1.8, it implements the general framework of Wood et al. (2016), which allows fitting GAMLSS models and using response distributions beyond the exponential family. However, the increased flexibility and scalability of `mgcv`'s model fitting methods has not been matched by the development of adequate visual tools for checking and exploring the model output. The `mgcViz` package is meant to fill this gap, by offering scalable and interactive visual tools for GAM visual model development and results presentation.

Most of the visual tools in `mgcv` are implemented by two functions: `plot.gam`, which plots the smooth effects or parametric terms, and `gam.check`, which performs model checking. Rather than providing few multiple purpose functions, `mgcViz` exploits the additive structure of GAMs to set up a modular and extensible object-oriented framework, which we briefly outline here. To provide a concrete example, let `obj` be an object of class `gamViz`, that is a GAM model fitted using the `gamV` function in `mgcViz`. Then the  $k$ -th fitted smooth or random effect contained in `obj` can be extracted using `ek<-sm(obj,k)`, and then transformed into a visual object of class `plotSmooth` by using `plot(ek)`. The generic `plot` function calls a specific plotting method, depending on the class of the effect considered. Parametric terms can be extracted using the `pterm` function, and can then be plotted similarly.

Most of the graphical objects produced by `mgcViz` belong to the `plotSmooth` class, which can be seen as a wrapper around an object of class `ggplot`, defined in the `ggplot2` package (Wickham, 2009). This allows us to exploit the powerful layering system provided by `ggplot2`, which enables users to superpose several graphical layers, possibly based on different data, on a single plot (Wickham, 2010). For example, assume that the effect `ek` extracted above is standard one-dimensional smooth, in which case we could do

```
plot(ek) + l_dens(type = "cond") + l_fitLine() + l_ciLine(linetype = 2)
```

which plots the fitted smooth effect with 95% confidence intervals, over a background heatmap representing the conditional density of the partial residuals (for an example of the latter, see Figure 1a). In `mgcViz` all functions with prefix `l_` output graphical layers, which can be added to the effect plots by using the overloaded `+` operator. One advantage of this system, relative to using few multiple purpose plotting functions, is that it can be extended easily by adding new layering methods. Secondly, most graphical and algorithmic parameters are specified directly at the level of the individual layers, allowing for more control than the current plotting methods provided by `mgcv`. Thirdly, basing the plotting system around `ggplot` objects allows us to exploit the vast array of layers provided by `ggplot2` and to convert (in an automatic fashion) the effect plots to `plotly` objects, which provide interactive features such as zooming and sub-setting, useful for exploring the model output and for model checking purposes.

In the rest of this section we describe several new methods for GAM model checking and smooth effect visualisation. Each time we describe a visual tool, we describe its mathematical and algorithmic structure, and we provide a reference to its implementation in `mgcViz`. This is because, while each new visualisation is useful individually, we argue that the layered object-oriented framework just outlined, and made available by `mgcViz`, is essential for creating an extensible, user-friendly and easily maintainable visual toolbox for GAM modelling.

## 2.2 Scalable interactive QQ-plots for general GAMs

Our aim here is developing QQ-plot methods for GAMs that are sufficiently fast to permit interactive exploration even for large data sets, that provide non-asymptotic confidence bands around the QQ-curve and that generalise to almost any response distribution.

Consider a data set consisting of covariate vectors  $\mathbf{x}_1, \dots, \mathbf{x}_n$  and responses  $y_1, \dots, y_n$ , distributed according to  $p(y|\mathbf{x})$ . For simplicity, assume that  $\mathbf{x} \in \mathbb{R}^d$ . Let  $p_m(y|\mathbf{x})$  be the model-based conditional distribution, and define the residuals  $r_i = t(y_i|\mathbf{x}_i)$ , for  $i = 1, \dots, n$ , where  $t(y|\mathbf{x})$  is a general sequence of transformations. Define the marginal distribution  $p(r) = \int p(r|\mathbf{x})p(\mathbf{x})d\mathbf{x}$  and its model-based estimate  $\hat{p}_m(r) = n^{-1} \sum_i p_m(r|\mathbf{x}_i)$ . Notice that, while  $p_m(r|\mathbf{x})$  depends only on the model and on  $t(y|\mathbf{x})$ ,  $p(r|\mathbf{x})$  depends also on the data generating process. In a regression context, QQ-plots are typically used to compare the quantiles of  $\hat{p}_m(r)$  with those of  $p(r)$ . The latter are typically unavailable, but can be estimated using the sample  $r_i \sim p(r)$ , for  $i = 1, \dots, n$ .

The main factors determining the facility with which the objectives stated above can be achieved are the transformation of interest and the tractability of  $p_m(y|\mathbf{x})$ . Commonly used transformations  $t(y_i|\mathbf{x}_i)$  are:

- (a)  $F_m(y_i|\mathbf{x}_i)$ , where  $F_m(y|\mathbf{x})$  is the conditional c.d.f. corresponding to  $p_m(y|\mathbf{x})$ .
- (b)  $\Phi^{-1}\{F_m(y_i|\mathbf{x}_i)\}$ , where  $\Phi$  is a standard normal c.d.f.. These are the ‘quantile’ residuals of Dunn and Smyth (1996).
- (c)  $\{y_i - \mu_m(\mathbf{x}_i)\}/\sqrt{v_m(\mathbf{x}_i)}$ , where  $\mu_m(\mathbf{x})$  and  $v_m(\mathbf{x})$  are model-based estimates of, respectively,  $\mathbb{E}(y|\mathbf{x})$  and  $\text{var}(y|\mathbf{x})$ . This produces scaled Pearson residuals.
- (d)  $\text{sign}\{y_i - \mu_m(\mathbf{x}_i)\}\sqrt{d_i}$ , where  $d_i$  is the  $i$ -th deviance component. This choice leads to the deviance residuals.

Leaving aside the sampling variability of the estimated model coefficients, and under a continuous  $y$  and a well specified model, options (a) and (b) should produce residuals that are, respectively, close to uniformly and normally distributed. In either case, the leading cost of computing the observed quantiles is  $O(n \log n)$ , if the  $r_i$ s are sorted sequentially. Under (a) confidence intervals (c.i.) can be obtained using the critical regions of the Kolmogorov-Smirnov statistic (Michael, 1983) while, under (b),  $\alpha\%$  c.i. around a normal quantile  $z$ , associated with probability  $p$ , can be approximated using  $\pm \Phi^{-1}\{(1 + \alpha)/2\}\phi(z)^{-1}\{p(1 - p)/n\}^{1/2}$ , where  $\phi$  is a standard normal p.d.f. (Buuren and Fredriks, 2001).

The plots obtained using residuals types (a) and (b) achieve the first two objectives stated above, but are difficult to interpret when the response variable takes few discrete values. Dunn and Smyth (1996) obtain continuous quantile residuals by randomising the uniform residuals  $F_m(y_i|\mathbf{x}_i)$ , and then transforming them to normality. Their method is simple and computationally cheap, but we are unsure about whether the randomisation affects the validity of confidence intervals derived as above. Scaled Pearson and deviance residuals are generally continuous even when the response is discrete and are arguably more popular than uniform or quantile residuals, in a regression context. While, under a general response distribution, not much can be said about the distribution of Pearson residuals, Pierce and Schafer (1986) argue that deviance residuals are generally close to normally distributed, in an exponential family context. However, there are cases of practical importance, such as when the response consists of low counts, where the resulting QQ-plots shows deviations from a straight line, even when the model is correct (Ben and Yohai, 2004). The `qq.gamViz` method in `mgcViz` addresses this issue by adopting the simulation-based approach of Augustin et al. (2012). Briefly, it simulates responses from the model, transforms them to residuals, and compares the observed ordered residuals with their simulated model-based counterparts. The advantage of this method is that it is very general (e.g. it can be applied to Pearson residuals) and that c.i. for the model-based quantiles can be estimated using the simulations. However, the leading cost of computation becomes  $O(mn \log n)$ , where  $m$  is the number simulated data sets used. Fortunately, the  $m$  iterations are independent and thus easy to parallelise.

Under residual types (a) and (b) `qq.gamViz` requires few seconds to calculate the QQ-curve and its c.i., for data sets of size  $10^7$  on a single core. In a similar setting and with  $m = 100$ , the simulation-based methods of Augustin et al. (2012) might take few minutes to produce the same output. The speed of the simulations could be improved, but at the time of writing this performance seems acceptable, if compared with the time needed to fit a GAM model to such a large data set. However, once the QQ-plot has been computed, it needs to be rendered graphically. Over-plotting is not an issue for QQ-plots, but R plotting facilities slow down considerably for  $n > 10^6$ , which impedes performing interactive actions on the plot. We address this problem by binning the points forming the QQ-plot and its c.i. before rendering. In particular, we construct  $b_0$  bins along the QQ-curve, with each bin covering the same arc-length. The arc-length of the original QQ-curve is  $l = \sum_{i=2}^n \{(r_i - r_{i-1})^2 + (\bar{r}_i - \bar{r}_{i-1})^2\}^{\frac{1}{2}}$ , where the  $r_i$ 's and  $\bar{r}_i$ 's are the sorted observed and model-based residuals. Having defined  $b_0$  bins along  $l$ , we attribute each point to a unique bin, and average the  $r_i$ 's and  $\bar{r}_i$ 's belonging to each bin. The output are two sequences  $s_j$  and  $\bar{s}_j$  with  $j = 1, \dots, b$ , where  $1 \leq b \leq b_0$  because some of the bins might be empty.

The cost of binning is  $O(n)$  or  $O(mn)$  if one wants to plot all the simulated QQ-lines. Notice that, with  $n = 10^7$  and  $m = 10^2$ , the latter option would require plotting  $10^9$  points if binning is not used, which is infeasible even for non-interactive use. For data sets of this size binning takes less than a second, which permits interactive features such as zooming. In `mgcViz` interactive zooming is provided by the `shine.qqGam` method, which transforms the output of `qq.gamViz` into a Shiny application (Chang et al., 2018). This interactive feature can be used to look at specific parts of the QQ-plot, without paying again the  $O(n \log n)$  price implied by sorting. Adapting the bins to the new zooming area allows the

user to check whether binning has hidden any feature of the original QQ-plot.

## 2.3 Beyond QQ-plots: conditional residual checks

The QQ-plot methods described in Section 2.2 focus on the marginal distribution of the residuals. Here we describe tools for assessing departures from the model-based conditional residuals distribution, along one or several covariates. Let  $x_j$ , with  $j \in \{1, \dots, d\}$ , indicate the  $j$ -th covariate and let  $x_{ij}$ , for  $i = 1, \dots, n$ , be its observed values. Plotting the residuals against the  $j$ -th covariate allows visualisation of a sample from  $p(r|x_j) = \int p(r|\mathbf{x})p(\mathbf{x}_{-j})d\mathbf{x}_{-j}$  which, in a classical regression context, helps identifying outliers, important omitted variables, non-linearities, heteroscedasticity and autocorrelations (Cox and Snell, 1968). When working with general GAMs, such plots can also help assessing over or under-smoothing and can prompt the addition of effects that let the skewness or tail behaviour of the response distribution vary with the covariates.

`mgcViz` provides several methods for comparing the observed and model-based conditional distributions of the residuals. At the time of writing the checks can be performed across either one or two covariates, but in principle they could be extended to any number of them. The implementation of these checks follows the layered framework described in Section 2.1. In particular, consider a fitted GAM model contained in an object `obj` of class `gamViz`. The function calls `check1D(obj, "x1")` and `check2D(obj, "x1", "x2")` can be used to extract the residuals from fitted GAM model, and to create graphical objects representing the relation between the residuals and the covariates  $x_1$  and  $x_2$ . Then visual residuals diagnostics can be plotted by adding one or more of the layers described in the following.

The `1_densCheck` layer produces a heatmap representing the distance,  $\delta_{p,p_m}(r|x_j)$ , between  $p(r|x_j)$  and  $p_m(r|x_j)$ . The user can provide any distance function, and Figure 1c-d shows two examples where  $\delta_{p,p_m}(r|x_j) = \{p(r|x_j)^{1/2} - p_m(r|x_j)^{1/2}\}^{1/3}$ .  $p(r|x_j)$  is estimated using  $p(r|x_j) = p(r, x_j)/p(x_j)$ , where fast kernel density estimates of  $p(r, x_j)$  and  $p(x_j)$  are computed using the `KernSmooth` package. This implements linear binning in one or two dimensions (Wand, 1994), hence it scales well with  $n$ . In Figure 1c-d  $p_m(r|x_j)$  is analytically available but, when it is not, it is possible to simulate residuals from the model and to use them to estimate  $p_m(r|x_j)$ , as done for  $p(r|x_j)$ .

Plotting  $\delta_{p,p_m}(r|x_j)$  provides much detail regarding the residuals distribution, but practitioners are often interested in specific residuals patterns (e.g. heteroscedasticity). Such focused checks can be performed using the `1_gridCheck1D` layer. This function attributes each residual to one of  $b$  bins, equally spaced along  $x_j$ , and summarises the residuals in each bin using a scalar valued function. Then it plots the summaries  $s_1, \dots, s_b$  against  $x_j$  (averaged within each bin). Confidence intervals can be obtained by simulating residuals from the model and summarising them. Figure 1e-f and 2f-g provide examples where the residuals are summarised using either the sample s.d. or the sample skewness. The `1_gridCheck2D` layer extends this approach to two dimensions. In particular, the observed and simulated residuals are binned and summarised using a 2D grid of bins. We use hexagonal bins because of their favourable visual properties (see e.g. Carr et al. (1987)). The variability of the observed patterns can be taken into account by standardising the sum-

maries based on the observed residuals using those based on the simulations, as done to obtain Figure 2d-e. Notice that these checks require only the ability to simulate responses from the model.

Binned residuals do not necessarily have to be reduced to scalar-valued summaries. For example, in Figure 4a the output of `l_gridCheck2D` has been overlaid with a grid of worm-plots (detrended QQ-plots meant to aid visibility of deviations from the horizontal line (Buuren and Fredriks, 2001)), while Figure 4b includes a sequence of kernel density estimates based on a coarser binning of the residuals. The `l_glyphs2D` layer allows users to summarise the residuals and the corresponding covariate values using any vector valued function, whose output can then rendered as a grid of glyphs. Wickham et al. (2012) point out that such glyph-maps are particularly useful for visualising spatio-temporal data but, as we show here, they can be used as residual checking tools, especially handy when assessing complex smooth interactions.

## 2.4 Visualising smooth effect uncertainty

Visually representing the uncertainty of the fitted smooth effects is important for communicating the results of a GAM-based statistical analysis, but this is not trivial to do when dealing with multi-dimensional effects. Here we propose several methods that allow visual assessment of the significance and uncertainty of bivariate smooths, and that could be extended beyond 2D. The first approach consists in letting the heatmap’s opacity be proportional to the significance of the fitted smooth at each location. Let  $\hat{f}_{x_1x_2} = \hat{f}(x_1, x_2)$  be the fitted smooth and  $\hat{v}_{x_1x_2} = \text{var}(\hat{f}_{x_1x_2})$  be its estimated variance. We determine the opacity using  $\alpha_{x_1x_2} = t\{\Phi(|\hat{f}_{x_1x_2}|/\sqrt{\hat{v}_{x_1x_2}})\}$ , where  $\Phi$  is a standard normal c.d.f. and  $t(p) : (0, 1) \rightarrow (0, 1)$  is a non-increasing transformation. Figure 5 uses  $t(p) = \max\{(1 - z)^\gamma, \beta\}$ , where  $z = \max(0, p - \delta)$ ,  $\delta = 0.05$ ,  $\gamma = 3$  and  $\beta = 0.2$ . Varying the opacity allows identification of areas where the smooth effect is significantly different from zero, but it is not always effective for visualising the uncertainty of  $\hat{f}_{x_1x_2}$ . This is better achieved by perturbing  $\hat{f}_{x_1x_2}$  using Gaussian white noise, with variance equal to  $\hat{v}_{x_1x_2}$ . The result is that the heatmap’s colours (see e.g. Figure 5) are proportional to the noisy function  $g_{x_1x_2} = \hat{f}_{x_1x_2} + z_{x_1x_2}$ , where  $z_{x_1x_2} \sim N\{0, \hat{v}_{x_1x_2}\}$ . One advantage of the methods just described is that significance and uncertainty are not presented in a binary ‘in-or-out’ fashion, as is typically the case when using fixed significance levels or confidence bands, which helps conveying the meaning of statistical uncertainty. Further, the introduction of an additional dimension is avoided.

A different approach to visual uncertainty quantification is 3D rendering of the smooth effects. `mgcViz` offers this feature via the generic `plotRGL` function, which uses the 3D interactive graphics offered by the OpenGL library (Neider et al., 1993), made accessible from R by the `rgl` package (Murdoch, 2001). Figure 6 shows a snapshot of an `rgl` graphic, which allows interactive manipulation (e.g. rotation and zooming) of each plot in the array. The plots use transparency to make both the fit and the confidence surfaces visible and include residuals (with sign-dependent colours), useful for diagnostic purposes. Here interactivity is essential: such 3D objects are more valuable than the 2D equivalents only if they can be manipulated in real time.

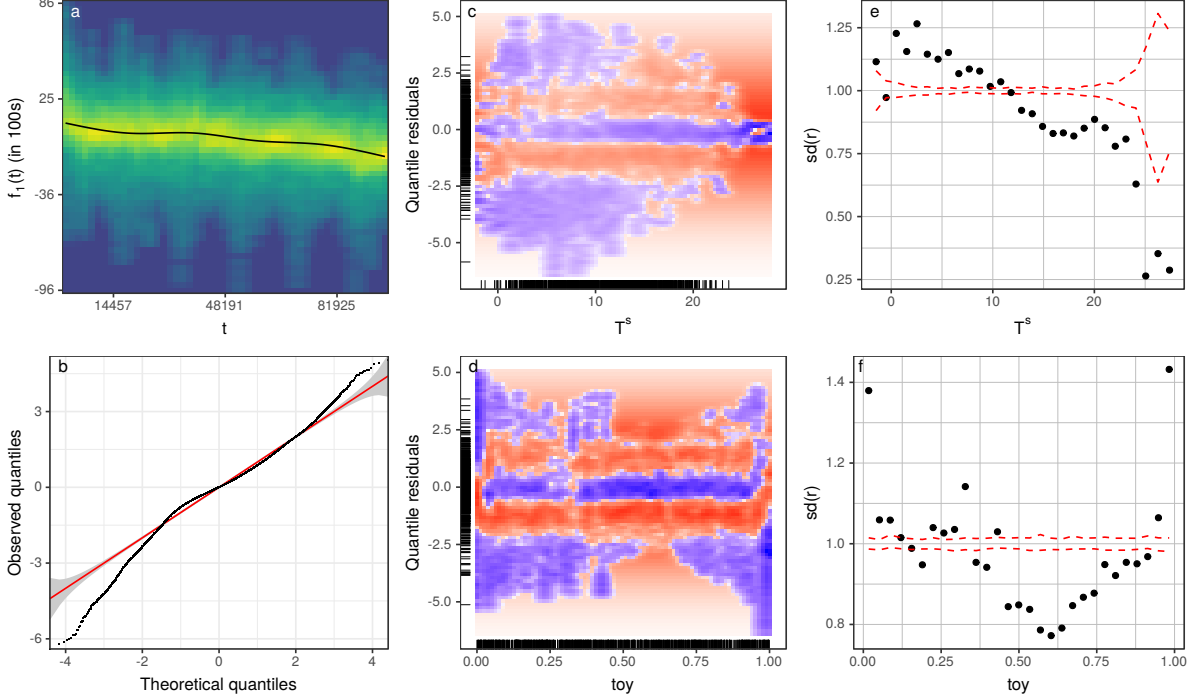


Figure 1: Gaussian GAM model. a)  $\hat{f}_1(t)$  and heatmap representing the conditional density of the partial residuals; b) normal QQ-plot with 99% c.i.; c) heatmap of  $\{p(r|T^S)^{1/2} - p_m(r|T^S)^{1/2}\}^{1/3}$ , based on a diverging red-blue palette; d) same for  $p(r|\text{toy})$ ; e-f) dots are the s.d. of the binned observed quantile residuals and the red lines are 90% c.i. based on  $m = 50$  simulated residuals vectors.

### 3 Interactive model building for electricity load forecasting

Rather than simply listing all the big data plot types developed (and implemented in `mgcViz`), here we present an illustration of the practical use of some key diagnostic plots in the context of building a GAM model for predicting electricity demand on the UK grid. Here ‘trying all possible models’ is clearly impossible and good visualisations are essential for interactive model building. The data, obtained from [www.nationalgrid.com](http://www.nationalgrid.com), covers the period between the 1st of January 2011 and the 30th of June 2016, and contains 48 daily observations of electricity load at half-hourly intervals. Hence, the data set amounts to a little less than  $n = 10^5$  observations. We integrate it with hourly temperatures obtained from the National Centers for Environmental Information (NCEI), covering the same period.

We start by considering a Gaussian GAM, where the model for expected load is

$$\mathbb{E}(L_i) = \beta_0 h_{d(i)} + \sum_{j=1}^7 \beta_j w_{d(i)}^j + \beta_8 L_{i-48} + f_1(t_i) + f_2(T_i, I_i) + f_3(T_i^s, I_i) + f_4(\text{toy}_i, I_i), \quad (1)$$

for  $i = 1, \dots, n$ . Here  $L_i$  is the  $i$ -th observed load,  $L_{i-48}$  is its value in the same half-hourly



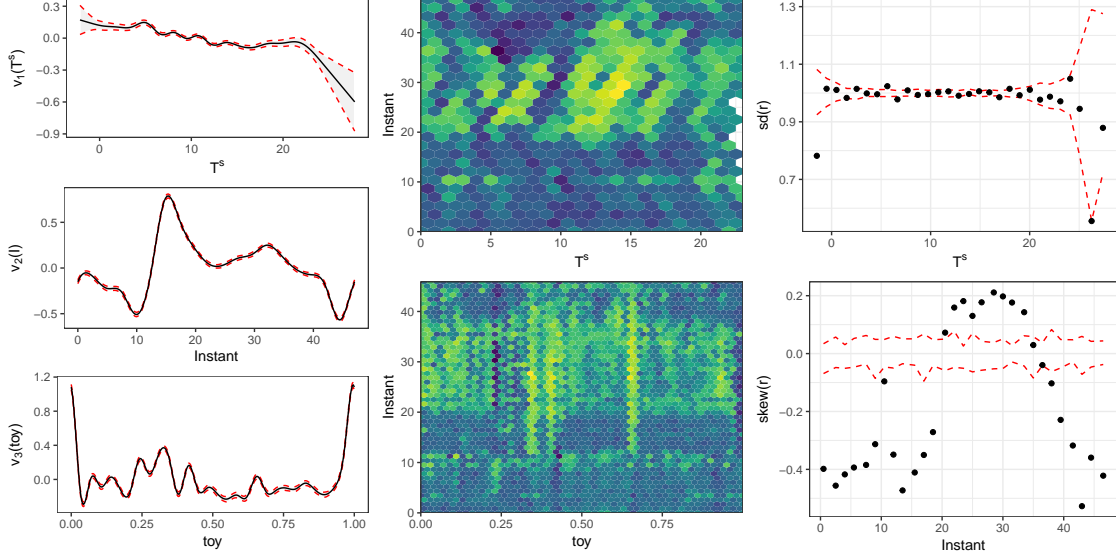


Figure 2: Scale-location model. a-c) smooth effects  $\hat{v}_1(T^s)$ ,  $\hat{v}_2(I)$  and  $\hat{v}_3(\text{toy})$ , with 95% c.i.; d) heatmap of s.d. of the observed quantile residuals in each bin, standardized using s.d. of  $m = 50$  residual vectors simulated from the model. e) same, but for sample skewness; f-g) analogous to Figure 1e-f, but here plot g uses sample skewness.

period of the previous day,  $d(i)$  is the corresponding date and  $h_{d(i)}$  is a binary variable equal to one if  $d(i)$  is a bank holiday, zero otherwise. Similarly,  $w_{d(i)}^j$  is equal to one if  $d(i)$  corresponds to the  $j$ -th day of the week, and  $\beta_0, \dots, \beta_8$  are unknown coefficients.  $t_i$  is time since the 1st of January 2011, and  $f_1$  is a smooth effect constructed using a cubic spline of rank six, meant to capture the long term trend.  $T_i$  and  $T_i^S$  indicate temperature and smoothed temperature, where the latter was obtained using  $T_i^S = \alpha T_i + (1 - \alpha)T_{i-1}^S$ , with  $\alpha = 0.95$ .  $I_i$  indicates the half-hour interval of the day, taking integer value between 1 and 48, and  $\text{toy}_i \in (0, 1)$  indicates the time of the year at half-hourly resolution.  $f_2$ ,  $f_3$  and  $f_4$  are bivariate smooth functions, based on tensor products of rank 200, 200 and 600. The tensor products are built using cubic spline marginal bases for  $T_i$  and  $T_i^S$ , and cyclic marginal bases for  $I_i$  and  $\text{toy}_i$ .

Figure 1 shows several diagnostics based on the quantile residuals (we will use this residual type throughout this section). The QQ-plot suggests that the residuals distribution  $p(r)$  is fat-tailed and left-skewed, and the remaining plots provide more detail regarding model mis-specification. In particular, the partial residuals density heatmap in 1a suggests the presence of a cyclical heteroscedastic component. This is confirmed by plot 1d, which shows that electricity demand is more variable in the winter than in the summer ( $\text{toy} \approx 0.7$ ). The plot also shows that the demand distribution is left-skewed during year-end, which is not surprising, given that UK consumption drops sharply in that period. Plot 1c shows that demand is more variable at low temperatures than at high temperatures, which is consistent with residential air conditioning being relatively uncommon in the UK. Plots 1e and 1f provide further evidence of heteroscedasticity along  $T^s$  and  $\text{toy}$ .

Plots 1c-d provide much detail regarding the residual conditional distribution, and thus

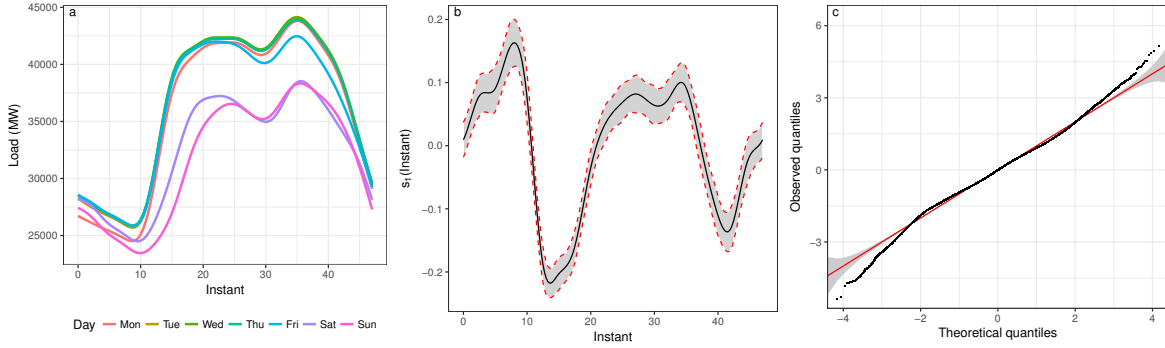


Figure 3: a) Daily load profiles, obtained by smoothing the load for each day; b) smooth effect  $\hat{s}_1(I)$  with 95% c.i.; c) QQ-plot of quantile residuals for the shash GAMLSS model.

are useful for detecting residuals anomalies. However, an advantage of plots 1e-f is that they include useful information on the significance of the observed heteroscedastic pattern. Further, focusing on specific features of the residual distribution, such as the conditional variance, is helpful during the GAM model development process. Indeed, plots 1e-f provide a strong case in favour of including effects that allow the variance to vary smoothly with  $T^s$  and  $\text{toy}$ . Analogous plots (not shown) suggest that the variance varies also with some of the remaining covariates, hence we model the scale as follows

$$g\{\text{sd}(L_i)\} = \alpha_0 h_{d(i)} + \sum_{j=1}^7 \alpha_j w_{d(i)}^j + v_1(T_i^s) + v_2(I_i) + v_3(\text{toy}_i), \quad (2)$$

where  $g(x) = \log(x - b)$  is a link function and  $b > 0$  is a small constant, included for computational stability reasons. The effects  $v_2(I)$  and  $v_3(\text{toy})$  are constructed using cyclic bases of rank 20 and 30, while  $v_1(T^s)$  is based on a cubic spline basis of rank 20.

The AIC of the resulting Gaussian location-scale model fit is  $1.62 \times 10^6$ , while that of the basic GAM is  $1.68 \times 10^6$ . Further, all the terms in model (2) have extremely low p-values ( $< 10^{-6}$ ). The temperature effect on load variance, shown in Figure 2a, implies that the variance decreases slightly with temperature, and 2f shows that the residual trend of 1e has now disappeared. The time of day effect is stronger, with the conditional variance being maximal at peak times. It is likely that  $v_2(I)$  is adjusting for the fact that the shape of the daily load profile changes depending on the day of the week, as illustrated by Figure 3a. Our mean model (1) includes a factor which simply shifts the profile curve depending on the day of the week. The discrepancy between the weekdays' and the Sunday's profiles reaches its peak around 8am, which is precisely the time at which the effect of  $I$  on the conditional variance is maximal. The effect of  $\text{toy}$  on the variance increases drastically near year-end. In part this is due to the mean model not being able to capture the sudden decline in demand that occurs during this period. It might be possible to address this issue by adopting an adaptive spline basis (see e.g. Section 5.3.5 of Wood (2017)), but this would lead to an overly complex model, as  $\text{toy}$  is part of a tensor product smooth.

The location model contains three bivariate smooths, hence it is reasonable to check for interactions acting on the conditional variance. Plot 2d shows one such check, which

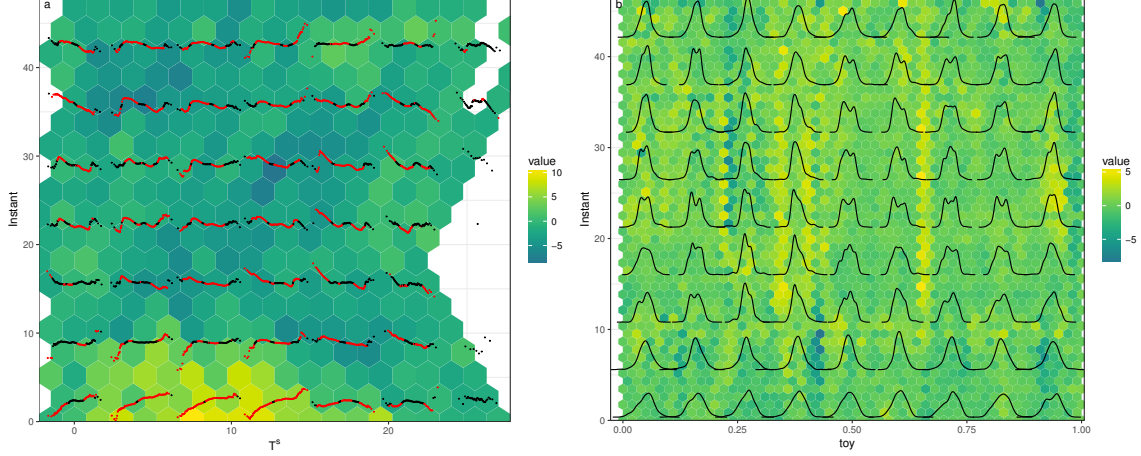


Figure 4: GAMLSS model. As in Figure 2d-e bin colours are computed using standardised s.d. (a) and skewness (b) in each bin. a) also shows several residual worm-plots, obtained using a coarser binning. Worms sections are red (black) if they fall outside (inside) 95% c.i.. b) uses the binned residuals to compute a grid of kernel density estimates.

gives no clear evidence favouring the addition of an interaction term in model (2). Figure 2e instead focuses on the skewness of the residuals across  $\text{toy}$  and  $I$ . It shows a broad horizontal stripe of high skewness, roughly covering the period 10am to 7pm, and several thin vertical patterns. The first pattern suggests that the model should include a smooth effect modelling skewness along  $I$ . Figure 2g provides further support for this. In contrast the vertical pattern is too irregular to be modelled effectively via a smooth effect along  $\text{toy}$ . Further, careful examination reveals that the vertical stripes correspond to variance peaks in plot 2c. We suspect that the variance and skewness patterns along  $\text{toy}$  could be reduced by more careful modelling of holiday periods in the mean model (1).

Further plots analogous to 2g (not shown) suggest the adoption of a GAMLSS model where the skewness depends on  $I$ , on the day of the week and on the holiday dummy variable. We base such model on the sinh-arcsinh (shash) distribution of Jones and Pewsey (2009), which has four parameters  $\mu$ ,  $\sigma > 0$ ,  $\epsilon$  and  $\delta > 0$  controlling location, scale, skewness and kurtosis. The model allows for skewness to either side, depending on the sign of  $\epsilon$ , and can have tails that are lighter ( $\delta > 1$ ) or heavier ( $0 < \delta < 1$ ) than a normal. We model  $\mu$  and  $\sigma$  using models (1) and (2), while for  $\epsilon$  we use

$$\epsilon_i = \gamma_0 h_{d(i)} + \sum_{j=1}^7 \gamma_j w_{d(i)}^j + s_1(I_i), \quad (3)$$

where  $s_1(I_i)$  is a smooth effect, constructed using a cyclic spline basis of rank 20. Despite having experimented with several transformation and link functions, we were unable to identify  $\delta$ . In particular,  $\delta$  was often diverging toward high values, where the density becomes insensitive to this parameter (Jones and Pewsey, 2009). Hence, we preferred fixing  $\delta$  to 1, which results in a GAMLSS model containing 1014 regression coefficients and 11 smoothing parameter. The increase in complexity seems justified, as the AIC of the

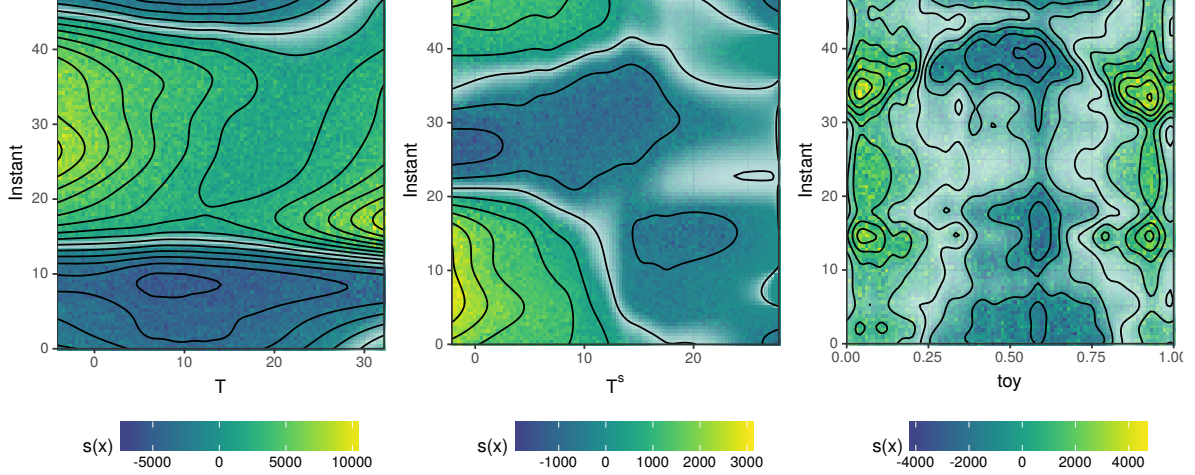


Figure 5: Smooth effects  $\hat{f}_1(T, I)$ ,  $\hat{f}_2(T^s, I)$  and  $\hat{f}_3(\text{toy}, I)$ , under the shash model. We use randomisation and transparency to quantify their uncertainty and significance.

shash model is  $1.608 \times 10^6$  and all of the terms in (3) are significant at 0.01 level.

Figure 3b shows that the shape of  $s_1(I)$  is roughly consistent with the skewness pattern observed in Figure 2e. The QQ-plot in Figure 3 is much improved relative to the one shown in Figure 1, especially in the lower tail. Fitting the four-parameters shash density to the residuals of the shash GAMLSS model returns  $\hat{\delta} \approx 1$  and an almost identical QQ-plot, suggesting that we have not lost much by fixing  $\delta$ . Still, the QQ-plot indicates that the fit could be improved further. Figure 4 provides more evidence of this. In particular, the worm-plots in 4a show large deviations of quantile residuals from normality, particularly in the lower tail. Further, the heatmap shows that the residuals are over-dispersed between midnight and 2am but not before midnight, which suggests that using a cyclic basis for  $v_2(I)$  might not be appropriate. The binned density estimates in Figure 4b show clear evidence of multimodality, which might be attributable to the shape of daily load profile being different depending on day of the week and to the fact that our model does not integrate special tariff information.

Figure 5 shows the bivariate smooth effects for the location parameter  $\mu$ . As expected the effect of variations in the instantaneous temperature  $T$  is much stronger during the day, due to manual or automated heating regulation. In contrast, low  $T^s$  has a strong positive effect at night, probably because of storage heaters. Notice that the effect  $\hat{f}_2(T^s, I)$  is barely significant for  $T^s > 20$ , as UK temperatures rarely stay much above 20°C for several consecutive days. The effect  $\hat{f}_3(\text{toy}, I)$  is quite complex and it is characterised by higher uncertainty. It shows four maxima, corresponding to daily peak times, separated along  $\text{toy}$  by the year-end demand drop. Figure 6 shows the same effects in three dimensions. Each plot includes a sub-sample of the residuals, with colours indicating whether they are positive (blue) or negative (red). The effect  $\hat{f}_3(\text{toy}, I)$  is presented from two different viewpoints, which show that this effect is much smoother across  $I$  than  $\text{toy}$ .

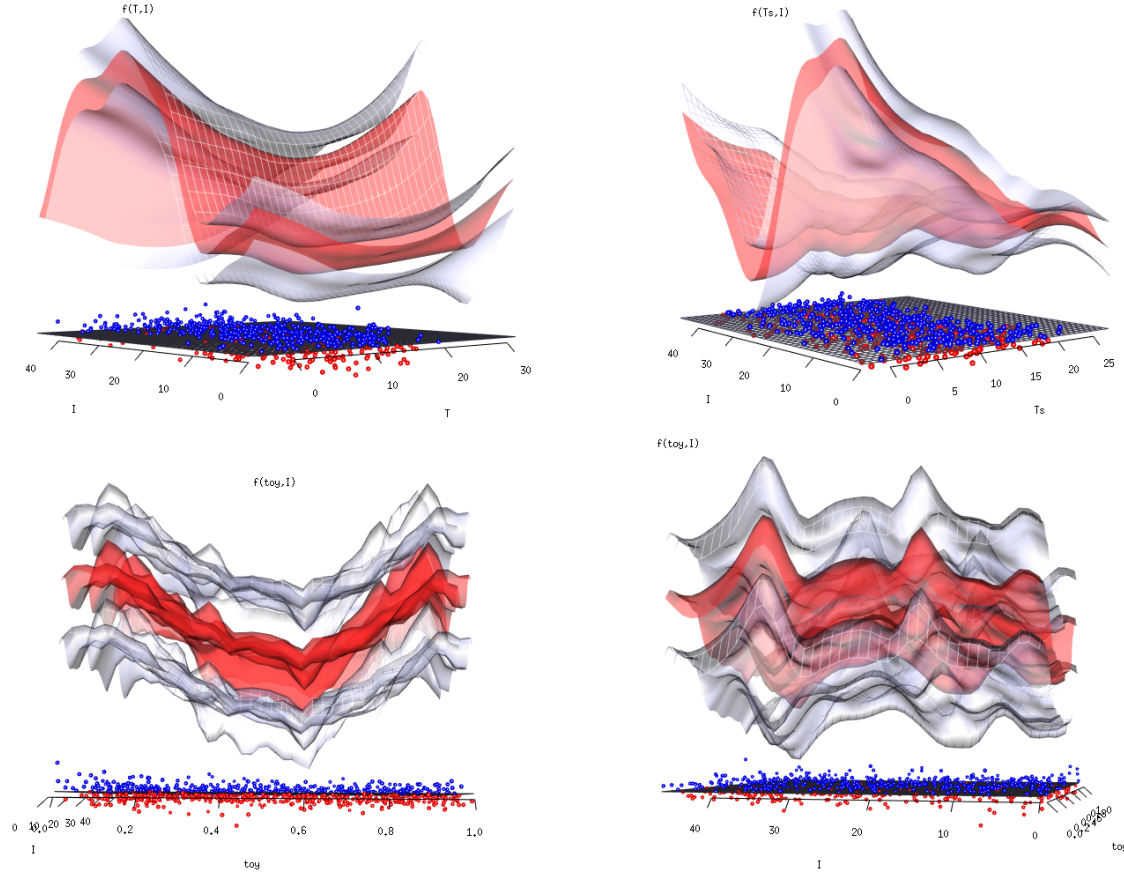


Figure 6: Snapshot of an `rgl` graphic showing  $\hat{f}_1(T, I)$ ,  $\hat{f}_2(T^s, I)$  and  $\hat{f}_3(\text{toy}, I)$ , under the shash model. The fitted effects are red, and 66% confidence surfaces are showed in grey.

## 4 Conclusions

We presented a set of scalable visual tools meant to facilitate results presentation, model checking and building for general GAMs. In the example we emphasised the use of visual aids for interactive model building, because we feel that this approach is much preferable to automated variable selection approaches when dealing with large data sets and complex models. Further, such visual checks allow practitioners to understand why an effect was included and thus to develop more confidence in the chosen model. This is key to fostering the adoption of more sophisticated GAM models in large industrial institutions, such as Électricité de France, where forecasting errors have major practical consequences.

## Acknowledgements

This work was funded by EPSRC grants EP/K005251/1 and EP/N509619/1. The first author was also partially supported by EDF.

## References

- Augustin, N. H., Sauleau, E.-A., and Wood, S. N. (2012) On quantile quantile plots for generalized linear models, *Computational Statistics & Data Analysis*, **56**, 2404–2409.
- Ben, M. G. and Yohai, V. J. (2004) Quantile–quantile plot for deviance residuals in the generalized linear model, *Journal of Computational and Graphical Statistics*, **13**, 36–47.
- Buuren, S. v. and Fredriks, M. (2001) Worm plot: a simple diagnostic device for modelling growth reference curves, *Statistics in medicine*, **20**, 1259–1277.
- Carr, D. B., Littlefield, R. J., Nicholson, W., and Littlefield, J. (1987) Scatterplot matrix techniques for large n, *Journal of the American Statistical Association*, **82**, 424–436.
- Chang, W., Cheng, J., Allaire, J., Xie, Y., and McPherson, J. (2018) *shiny: Web Application Framework for R*, r package version 1.1.0.
- Cox, D. R. and Snell, E. J. (1968) A general definition of residuals, *Journal of the Royal Statistical Society. Series B (Methodological)*, pp. 248–275.
- Dunn, P. K. and Smyth, G. K. (1996) Randomized quantile residuals, *Journal of Computational and Graphical Statistics*, **5**, 236–244.
- Jones, M. and Pewsey, A. (2009) Sinh-arcsinh distributions, *Biometrika*, **96**, 761–780.
- Michael, J. R. (1983) The stabilized probability plot, *Biometrika*, **70**, 11–17.
- Murdoch, D. (2001) Rgl: An r interface to opengl, in *Proceedings of DSC*, p. 2.
- Neider, J., Davis, T., and Woo, M. (1993) OpenGL programming guide.
- Pierce, D. A. and Schafer, D. W. (1986) Residuals in generalized linear models, *Journal of the American Statistical Association*, **81**, 977–986.
- Rigby, R. A. and Stasinopoulos, D. M. (2005) Generalized additive models for location, scale and shape, *Journal of the Royal Statistical Society: Series C*, **54**, 507–554.
- Wand, M. P. (1994) Fast computation of multivariate kernel estimators, *Journal of Computational and Graphical Statistics*, **3**, 433–445.
- Wand, M. P. (2017) Fast approximate inference for arbitrarily large semiparametric regression models via message passing, *Journal of the American Statistical Association*, **112**, 137–168.
- Wickham, H. (2009) *ggplot2: Elegant Graphics for Data Analysis*, Springer-Verlag New York.
- Wickham, H. (2010) A layered grammar of graphics, *Journal of Computational and Graphical Statistics*, **19**, 3–28.



- Wickham, H. (2013) Bin-summarise-smooth: a framework for visualising large data, *had.co.nz, Tech. Rep.*
- Wickham, H., Hofmann, H., Wickham, C., and Cook, D. (2012) Glyph-maps for visually exploring temporal patterns in climate data and models, *Environmetrics*, **23**, 382–393.
- Wood, S. N. (2017) *Generalized additive models: an introduction with R*, CRC press.
- Wood, S. N., Goude, Y., and Shaw, S. (2015) Generalized additive models for large data sets, *Journal of the Royal Statistical Society: Series C (Applied Statistics)*, **64**, 139–155.
- Wood, S. N., Pya, N., and Säfken, B. (2016) Smoothing parameter and model selection for general smooth models, *Journal of the American Statistical Association*, **111**, 1548–1575.
- Wood, S. N., Li, Z., Shaddick, G., and Augustin, N. H. (2017) Generalized additive models for gigadata: Modeling the uk black smoke network daily data, *Journal of the American Statistical Association*, pp. 1–12.